Original paper

Ground Motion Prediction Model for Southeastern Mexico Removing Site Effects Using the Earthquake Horizontal-to-Vertical Spectral Ratio (EHVSR)

Javier F. Lermo-Samaniego*[1], Miguel A. Jaimes[1], Francisco J. Sánchez-Sesma[1], Cristian Campuzano-Sánchez[1], Hugo Cruz-Jiménez[1,3] and José Oscar Campos-Enriquez[2]

Received: September 23, 2019; accepted: April 22, 2020; published online: October 1, 2020

Resumen

Se propone un modelo de atenuación del movimiento del terreno (GMPE, por sus siglas en inglés) para el sureste de México. El modelo de atenuación es una función de la magnitud y distancia. Se utilizan 86 sismos con magnitudes $5.0 \leq M_w \leq 8.2$ (se incluyen registros del terremoto de Tehuantepec del 7/09/2017, Mw 8.2) y distancias epicentrales entre $52 \leq R \leq 618$ km. Los eventos se registraron en nueve estaciones de la red acelerométrica del Instituto de Ingeniería de la Universidad Nacional Autónoma de México (II-UNAM) instaladas en los estados de Chiapas, Oaxaca, Tabasco y Veracruz. Se estima el efecto de sitio de los registros sísmicos de estas estaciones mediante el cociente espectral promedio de los movimientos horizontales y el vertical de sismos (EHVSR, pos sus siglas en inglés).Se señala la necesidad de remover el efecto de sitio en los modelos actuales de atenuación del movimiento fuerte debido a que inducen sobreestimación de los sismos.

Palabras clave: GMPE para el Sureste de México, efecto de sitio, EHVSR.

Abstract

A ground motion attenuation model (ground motion prediction equation, GMPE) for southeastern Mexico is proposed. The attenuation model was built as a function of magnitude, and distance. A number of 86 earthquakes were used with $5.0 \leq Mw \leq 8.2$ (including the recordings of the 9/7/2017, Mw8.2 Tehuantepec earthquake), and distances between $52 \leq R \leq 618$ km. They were recorded in nine stations of the Engineering Institute of the National Autonomous University of Mexico (II-UNAM) accelerometric network installed in the states of Chiapas, Oaxaca, Tabasco and Veracruz. From all recordings of each of these stations, we removed site effects, which were estimated using the average Earthquake Horizontal to Vertical Spectral Ratio (EHVSR). This work points out the need to remove site effect in the current GMPEs, which tends to overestimate this effect.

Key words: Ground-Motion Prediction Equation (GMPE) for Southeast Mexico, site effect, EHVSR (Earthquake Horizontal to Vertical Spectral Ratio).

*Corresponding author: jlermos@iingen.unam.mx

1 Instituto de Ingeniería, Universidad Nacional Autónoma de México. Circuito Interior, Ciudad Universitaria, Coyoacán, 04510, CDMX, México

2 Instituto de Geofísica, Universidad Nacional Autónoma de México. Circuito Interior, Ciudad Universitaria, Coyoacán, 04510, CDMX, México.

3 Instituto de Ingeniería, Universidad Veracruzana, Boca del Río, Veracruz, México

Introduction

On September 7, 2017, a Mw8.2 earthquake took place in the Tehuantepec Gulf, 133 km to the southwest of Pijijiapan, Chiapas. This earthquake occurred at 23:49:18, local time (September 08, 2017; 04:49 UTM), localized by the National Seismological Service (SSN for Servicio Sismológico Nacional, in Spanish) at 14.85° N and 94.11° W, at a depth of 58 km (Figure 1). It caused major damage in southeastern Mexico, in particular in the states of Chiapas and Oaxaca (Special Report, SSN, 2017). Specific different conditions are associated with these two states. While in Oaxaca the damages are concentrated almost in the isthmus region municipalities, in Chiapas the effects are scattered, affecting 82 out of the 122 municipalities of this state, amounting more than a million people (HIC-AL, 2017).

In the last years, major progresses have been achieved in understanding the origin of the subduction and intraplate seismicity in central Mexico (i.e., García, 2007). For example, the advance in the knowledge of wave propagation from these events, as well as our capacity to estimate the ground motions due to such events. In contrast, the study of seismic events from the southeastern Mexico has been rather limited, in particular the region of the Tehuantepec Isthmus and the Chiapas State.

Southeastern Mexico is featured as a tectonically active zone associated with the interaction of the North American, Caribbean and Cocos tectonic plates. The first two plates are in lateral contact along the Polochic-Motagua Fault System. The Central America Volcanic Arc (AVCA; from the initials in Spanish) is due to the subduction of the Cocos plate beneath the North America to the north, and beneath the Caribbean plate to the south (Figure 1). This volcanic arc stretches more than 1,300 km from the Tacana active volcano, at the Mexico-Guatemala border, up to the Turrialba volcano in eastern Costa Rica. This subduction process in Mexico has given rise to the Chiapas Volcanic Arc (AVC; from the initials in Spanish) that irregularly extends in Chiapas up to El Chichón Volcano.

Pre-Mezosoic basement rocks are present in Central America (in Chiapas, Guatemala, Belice and Honduras). These rocks crop out south of the Yucatan-Chiapas block. The coast parallel Upper Precambrian-Lower Paleozoic Chiapas Massif covers a surface of more than 20,000 km^2, and constitutes the largest Permian crystalline complex in Mexico, comprising plutonic and metamorphic deformations (Weber *et al.*, 2006).

Three seismogenic sources feature this region. The first one is associated with the subduction of the Cocos plate beneath the North American plate (Figure 1). In this study it is considered that the contact between these two plates reaches a depth of 80 km (Figure 1, right panel). Kostoglodov and Pacheco (1999) analyzed six events from this source. They occurred on April 19, 1902 (M7.5), September 23, 1902 (M7.7), January 14, 1903 (M7.6), August 6, 1942 (M7.9), October 23, 1950 (M7.2), and April 29, 1970 (M7.3). For the September 23, 1902, and April 29, 1970 events, focal depths of 100 km beneath the Chiapas depression were reported by Figueroa (1973), which seems too large and probably related to scarce recordings. In the meantime, three major seismic events that took place in this region have been accurately localized by the SSN. These earthquakes are: September 19, 1993 (M_w 7.2) localized near Huixtla, Chiapas, with a focal depth of 34 km, November 7, 2012 (M_w 7.3), 68 km southwest of Ciudad Hidalgo, Chiapas, with a focal depth of 16 km and a reverse fault mechanism (severe damages affected San Marcos, Guatemala), and the Tehuantepec isthmus zone, September 7, 2017 (M_w 8.2), which constitutes the strongest historical earthquake recorded in Mexico, localized at 133 km southwest of Pijijiapan, Chiapas at a depth of 58 km. Its normal faulting focal mechanism adds to the controversy on the earthquakes of this region (an inverse faulting mechanism was expected). Also noteworthy is the number of aftershocks that amounted to 4,075 in 15 days, forming distributed clusters in all the Tehuantepec Gulf (special Report, SSN, Nov. 2017). Also contrasting are the observed peak accelerations. Even more, the peak accelerations at the horizontal components observed at the coast (NILT ~ 500 gals) contrast with the maximum values observed in stations located in the Chiapas depression (at stations TGBT and SCCB, values of ~ 300 ~ 100 gals, respectively). These contrasting values might be due to the Chiapas Massif that attenuates waves coming from the subduction zone. The second seismogenic source comprises the internal deformation of the subducted plate, and generates seismic events in a depth range between 80 and 250 km. An example is the October 21, 1995 (M_w 7.2) earthquake, localized 57 km from Tuxtla, Chiapas, at a depth of 165 km, which also shows variations in the peak accelerations observed at the recordings of this zone (Rebollar *et al.*, 1999). Another deep seismic event occurred on June 14, 2017 (M_w 7.0), located 74 km to the northeast of Ciudad Hidalgo, Chiapas, with a focal depth of 113 km. The third seismogenic source corresponds to a less than 50 km depth crustal deformation that comprises shallow faults. Approximately 15 faults produce the observed seismicity. The associated seismic events are of moderate magnitudes that cause local damages, as reported by Figueroa (1973). Examples from this third source are the swarms with peak M_c 5.5, that occurred in Chiapa de Corzo during July-October, 1975 (Figueroa *et al.*, 1975).

Considering the past seismic activity, here summarized, and the recent Tehuantepec earthquake (September 7, 2017, Mw8.2), it is of interest to analyze these seismic events to develop an attenuation model for the strong motion for southeastern Mexico (GMPE). In this study, based on the one stage maximum likelihood technique (Joyner and Boore, 1993), we developed empirical expressions to estimate the response spectra for the 5 per cent critical damping, peak ground acceleration (PGA), and peak ground velocity (PGV) for 86 seismic events.

As it is customary accepted, seismic ground motion can be roughly represented by three main factors: source, path, and site effects. This convolutional model is a crude approximation of reality, yet it is useful to assess significant characteristics of ground motion. The effects of surface geology, usually called site effects, can give rise to large amplifications and enhanced damage (see Sánchez-Sesma, 1987). In principle, transfer functions associated to sundry incoming waves with various incidence angles and polarizations can describe site effects. However, the various transfer functions are often very different partially explaining why the search for a simple factor to account for site effects has been futile so far. With the advent of the diffuse field theory (see Weaver, 1982; 1985; Campillo and Paul, 2003; Sánchez-Sesma *et al.*, 2011a), it is established the great resolving power of average energy densities within a seismic diffuse field. The coda of earthquakes is the paradigmatic example of a diffuse field produced by multiple scattering (see Hennino *et al.*, 2001; Margerin *et al.*, 2009). In a broad sense, this is the case of seismic noise (Shapiro and Campillo, 2004) and ensembles of earthquakes (Kawase *et al.*, 2011; Nagashima *et al.*, 2014; Baena-Rivera *et al.*, 2016). Therefore, according to Kawase *et al.* (2011) the EHVSR in a layered medium is proportional to the ratio of transfer functions associated to vertically incoming P and SV waves, without surface waves. Uniform and equipartitioned illumination give rise to diffuse fields (Sánchez-Sesma *et al.*, 2006). In irregular settings, multiple diffraction tends to favor equipartition of energy in the diverse states: P and S waves and sundry surface (Love and Rayleigh) waves. Sánchez-Sesma *et al.* (2011b) showed that by assuming a diffuse wave field, the NHVSR can be modeled in the frequency domain in terms of the ratio of the imaginary part of the trace components of Green's function at the source. This approach includes naturally the contributions from Rayleigh, Love and body waves.

In seismic zones, it seems reasonable to use recorded ground motions to compute the average energy densities of earthquake ground motions and assess by their ratios approximate average spectral realizations of site effects (Carpenter *et al.*, 2018). Therefore, the use of a binary variable is clearly very rough and does not account for the presence of dominant frequencies excited during earthquake shaking. The average EHVSR approximately accounts for this. The GMPE has a regional use and they should be free of site effects in order to avoid bias in the model. This research aim is to approximately remove this effect.

In order to evaluate seismic hazard, site effects have to be incorporated back correcting the GMPE using HVSR with the appropriate corrections as proposed by Kawase *et al.* (2018). Note that HVSR is a proxy of empirical transfer functions in low frequencies with obvious underestimations in higher frequencies. In fact, several authors have stated that, the noise HVSR spectral ratio (NHVSR) provides a reasonable estimate of the site dominant frequency (see Nakamura, 1989). However, its amplitude is subject of controversy (i.e., Finn, 1991; Gutiérrez and Singh, 1992; Lachet and Bard, 1994). In very soft sedimentary environments the NHVSR, the EHVSR and the theoretical transfer functions are in reasonable agreement in low and moderate frequencies (Lermo and Chávez-García, 1994b).

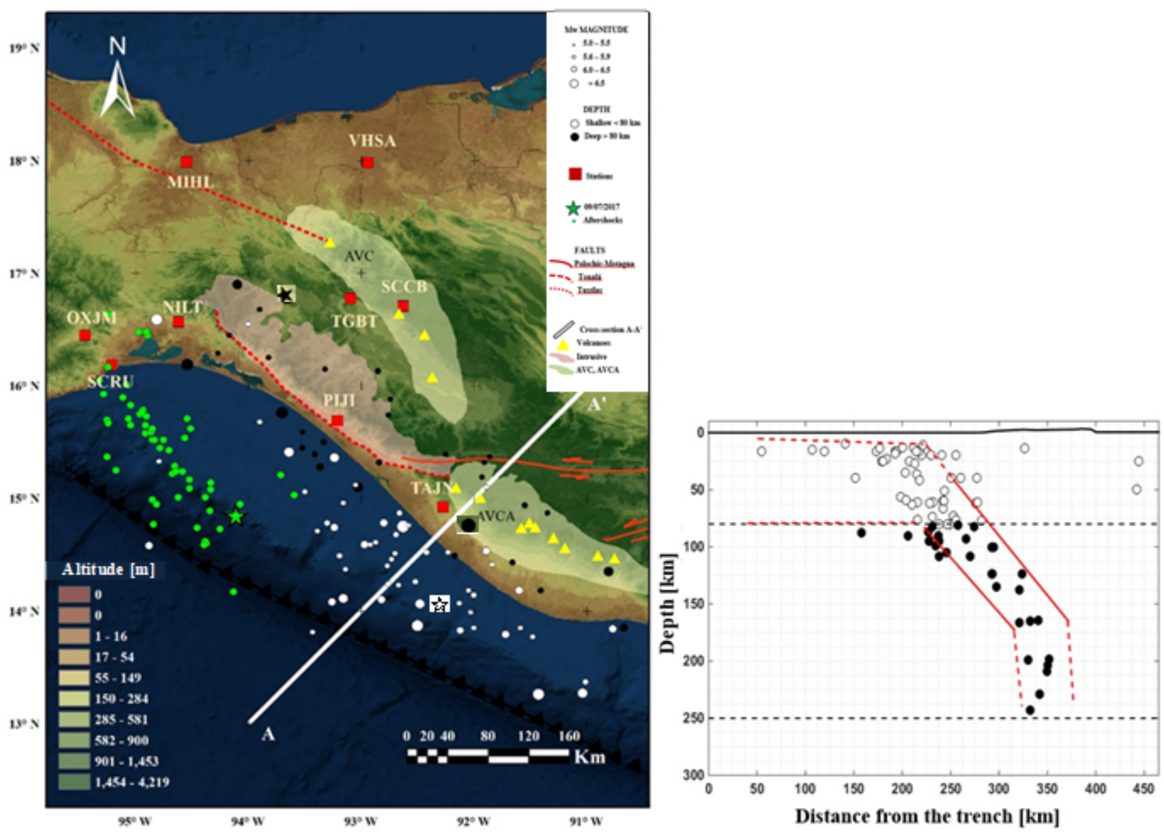

Figure 1. Left panel shows a map of the southeastern Mexico indicating the epicenters of earthquakes analyzed in this study (white and black circles), aftershocks of the September 8, 2017 earthquake (green circles), stations (red squares), volcanoes (yellow triangles) faults, an intrusive, as well as the Central America Volcanic Arc (AVCA; from the name in Spanish) and Chiapas Volcanic Arc (AVC; from the name in Spanish). The cross-section A-A' is also indicated. Right panel shows hypocenters projected on the A-A' cross-section. We separate hypocenters with depths shallower and deeper than 80 km (white and black circles, respectively).

Data

From the SSN database we selected 86 earthquakes (of various focal mechanism) located between 90.5° W and 96.5° W and between 13° and 17° N, and which occurred between 1995 and 2017. From this database, we present a wide range of magnitudes ($5.0 \leq Mw \leq 8.2$), distances ($52 \leq R \leq 618$ km; hipocentral distances for Mw<=7.0 and rupture distances for Mw> 7.0) and depths ($10 \leq H \leq 243$ km) as shown in Figure 1 and Table 1. We obtained 261 three-components accelerograms for those events recorded at 9 stations located in Chiapas, Oaxaca, Tabasco and Veracruz. The respective stations are OXJM, SCRU, NILT, MIHL, PIJI, TGBT, VHSA, SCCB and TAJN and belong to the Seismic Network of Institute of Engineering-UNAM (Pérez-Yáñez *et al.*, 2010). Date, depth, moment magnitude (Mw) and distance for each recording are indicated in Table 1. The farthest away stations (VHSA and MIHL) have less recordings, in contrast with those sited in the central part of the study area (PIJI, NILT, SCCB, OXJM, TAJN, TGBT and SCRU) where the Chiapas State capital city (Tuxtla Gutierrez) and the hidroelectric dams are located.

The spatial distribution of the 9 accelerometric stations (red squares), and of the 86 epicenters (white and black circles) is shown in Figure 1. Also indicated are the locations of the Chiapas (AVC) and Guatemala (AVCA) volcanic arcs. The Chiapas Massif is depicted in pink. Figure 1 also shows the Polochic-Motagua (continuous red line), Tonalá and Los Tuxtlas (discontinuous red line) fault systems. The epicenter of the Tehuantepec, September 7, 2017 (Mw8.2) earthquake is indicated with a green star. Green small dots represent aftershocks with magnitudes lower than 5. A comparison of the area covered by the aftershocks of the Tehuantepec earthquake with the localized seismicity of the last 17 years indicates that the Tehuantepec aftershocks cover that portion of the Tehuantepec Gulf that had been inactive.

In the right panel of Figure 1. The 261 hypocenters analyzed in this study were projected to the A-A´ cross-section (right panel of Figure 1), whose location is indicated with a white line. A dipping angle of the slab of about 45 degrees, as well as a plate thinning at 80 km depth can be observed.

Stars indicate the epicenters of the three earthquakes with Mw > 7.0 (see Table 1). For these events, the minimum distance to the rupture was considered. For the October 21, 1995 earthquake (Mw 7.2), according to the rupture model proposed by Rebollar *et al.* (1999), the rupture depth (htop) lies at 80 km. For the September 8, 2017 event (Mw 8.2), we used the rupture model obtained by Ye *et al.* (2017), which has a htop = 30 km. Finally, for the November 7, 2012 (Mw 7.3) event, for which there is no rupture model, we assumed a rupture model with a htop = 10 km, with its closest edge point (northwestern edge of the fault plane) at latitude 14º N and longitude 92º W.

Figure 2 shows the distribution of magnitudes ($5.0 \leq Mw \leq 8.2$) versus distance ($52 \leq R \leq 618$ km) of the analyzed records. A concentration of events with magnitudes in the range from 5.0 to 5.5 for distances between 52 and 300 km is observed.

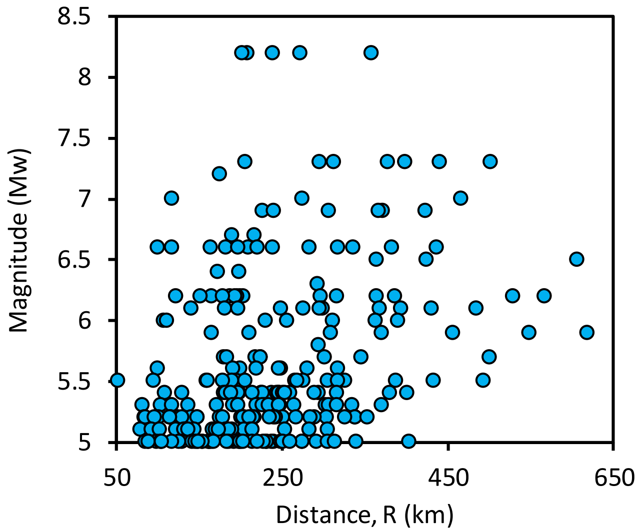

Figure 2.- Moment magnitude (Mw) distribution against distance of the analyzed seismic events.

DATA PROCESSING AND ANALYSIS

For each of the three components of the 261 recordings associated to the 86 selected seismic events, both shear waves and surface waves (also known as coda) were selected. Data processing included homogenization of the signal sampling of all extracted signals. Subsequently, for each selected record, the Fourier amplitude spectrum (FAS) was computed and the spectral ratio of horizontal components with respect to the vertical one obtained. After that, the quadratic means were obtained from both ratios. These are the directional earthquake horizontal to vertical spectral ratios (EHVSR), which were computed for a frequency band between 0.1 and 10 Hz. In Figure 3 we show the 261 ratios (thin of colors continuous lines) distributed in the 9 stations. Averages are depicted as continuous red lines (dashed red lines: average ± one standard deviation). We assume that this average of directional EHVSR´s is an estimate of the spectral amplification, a kind of empirical transfer function (ETF) of average horizontal components with respect to the vertical component. The source effect is approximately removed. In a recent paper, Kawase *et al.* (2018) suggested to consider the amplification due to vertical motion to avoid over-reduction of FAS. However, this requires recordings both in soil and rock sites.

It has been proposed that the site effect is significant for ETF larger than two (SESAME, 2015) as it is the case of scalar amplification in a half-space. However, under the assumption of a diffuse field, Sánchez-Sesma *et al.* (2011a) found theoretically that the MHVSR at the surface of a half-space is approximately given by

$$H/V \approx 1.245 + 0.348 \cdot \upsilon \qquad (1)$$

where υ=Poisson ratio. If υ =0.25 then the H/V is about 1.332.

Thus, according to criteria from SESAME (continuous line in Figure 3), and to that of Sánchez-Sesma *et al.* (2011) (discontinuous line in Figure 3), the 9 accelerometric stations present site effects in the analyzed frequency band. Stations NILT and PIJI reach amplifications of more than ten times at 6 and 4 Hz, respectively. Stations OXJM, SCRU and TGBT present lower amplifications.

Table 1. Earthquakes from southeastern Mexico analyzed in this study.

No.	Date (dd/mm/yy)	Lat (° N)	Lon (° W)	H* (km)	Mw	Distances of the records (km)* MIHL	NILT	OXJM	PIJI	SCCB	SCRU	TAJN	TGBT	VHSA
1	21/10/1995	16.92	93.64	165	7.2								92	
2	03/06/2000	15.76	-94.66	88	5		126				117			
3	12/03/2000	14.59	-92.97	35	5.9		165				308			
4	17/10/2000	15.38	-92.51	168	5.5		317							
5	09/01/2001	15.36	-93.24	66	6.1						248			
6	19/01/2001	15.1	-93.03	108	6.3						292			
7	28/11/2001	15.41	-93.64	36	6.4		172				198			
8	16/01/2002	16.59	-94.81	76	6.7		189				217			
9	14/02/2002	14.78	-92.8	74	5.8		293							
10	06/06/2006	15.37	-91.86	209	5				260			220		
11	13/06/2007	13.26	-91.43	20	6.6				336			208		
12	06/07/2007	16.9	-94.1	100	6.2	165	121	187	195	193	178	316	151	203
13	23/07/2007	14.18	-91.41	124	5.4				289					
14	30/08/2007	15.68	-93.9	61	5		141		98	192				
15	26/11/2007	15.28	-93.36	87	5.6		218	280	100	199	245		190	317
16	05/01/2008	13.83	-92.12	63	5.6				248					
17	06/01/2008	13.99	-92.03	20	5				231					
18	12/02/2008	16.19	-94.54	90	6.6	220	100		182	238	117		196	282
19	04/04/2008	13.85	-91.59	73	5.1				282					
20	15/04/2008	13.27	-91.04	40	6.5			606	364	424				
21	17/04/2008	15.45	-93.52	95	5.4		198	259		196	226		182	
22	20/09/2008	14.23	-92.67	14	5		339							
23	16/10/2008	13.87	-92.5	23	6.6		382	436		317				
24	17/01/2009	15.74	-92.76	171	5.2		284	353	178	203	326		210	
25	22/01/2009	15.19	-91.93	199	5				251					
26	03/05/2009	14.53	-91.89	77	5.9			456	210					
27	07/06/2009	16.15	-93.32	135	5		203	274	145	168	250		154	248
28	18/01/2010	13.85	-90.67	124	5.9		548	618	370					
29	23/02/2010	15.96	-91.22	25	5.4				225	180				
30	20/03/2010	16.03	-91.32	50	5.3				219	171				
31	19/08/2010	14.41	-91.84	40	5.2				212			85		
32	15/09/2010	15.59	-93.52	95	5.1		189	253	102	186			170	
33	01/11/2010	16.68	-93.9	124	5		148	214	183		199		154	
34	20/01/2011	16.55	-94	62	5.1	182	93	173	144	166			121	
35	27/03/2011	14.24	-92.76	16	5.5			387		276				
36	26/04/2011	15.88	-92.74	138	5				149					
37	07/06/2011	15.06	-93.5	56	5.2		216		96	215	235			
38	13/08/2011	14.58	-94.88	16	5.7		224	218	224	346				
39	06/09/2011	16.25	-93.82	93	5.1		133	205	131	170			137	
40	19/10/2011	15.12	-93.05	80	5		237	305	104	200				
41	17/11/2011	14.52	-92.42	20	5.5				158			52		
42	10/12/2011	15.33	-94.79	16	5.2		140							
43	20/12/2011	13.81	-93.43	15	5.1				211					
44	21/01/2012	14.74	-93.24	16	6	390	255	311	107	230		111		363
45	16/02/2012	14.59	-92.92	25	5		291		129	239		85		
46	20/02/2012	14.37	-93.14	16	5.2				148			116		
47	13/03/2012	14.96	-93.16	16	5.2		242	304	83	204	266	100	203	338
48	01/05/2012	14.11	-93.16	40	6.1				181	298		140		
49	26/06/2012	15.39	-92.25	166	5.2		338		200			174		
50	29/06/2012	14.78	-93.3	18	5.3			303	103	228		117		
51	12/07/2012	14.87	-91.35	204	5.1				305					
52	29/07/2012	14.1	-92.82	14	5.7				183					
53	01/09/2012	16.13	-92.85	243	5.4		316	379	251	253				
54	14/10/2012	14.46	-92.73	13	5.2				148	251				
55	15/10/2012	13.77	-91.48	20	5.2				288					
56	27/10/2012	14.4	-92.77	59	5				163					
57	07/11/2012	14.03	-92.32	16	7.3	519	400		230	309	422		330	453
58	11/11/2012	14.06	-92.48	13	6.2				199	296				
59	16/12/2012	14.43	-91.66	100	5.4				244					
60	30/12/2012	14.49	-93.19	25	5.3				136					
61	31/12/2012	15.21	-92.67	82	5.2				115					
62	11/01/2013	14.61	-92.87	27	5.4		293		129	237				
63	11/01/2013	15.32	-91.91	229	5		403		273					
64	25/03/2013	14.35	-90.81	198	6.2		529		364	386	567			
65	10/05/2013	14.87	-92.66	35	5.3				247					
66	30/07/2013	15.5	-93.33	105	5.4		214		108	189	246		246	246
67	06/08/2013	14.18	-91.6	61	5.7			501						
68	07/09/2013	14.34	-92.26	69	6.1	484	367	431	196	276	394		295	
69	07/09/2013	14.14	-92	51	5.4		401		225					
70	10/01/2014	14.52	-92.23	76	5							88		
71	11/01/2014	14.49	-92.17	81	5.5			432	194	265		95		
72	02/03/2014	14.08	-93.26	10	5.7				180	301				
73	16/06/2014	15.1	-91.89	14	5				161	197				
74	07/07/2014	14.75	-92.63	60	6.9	423	305	371		226			239	367
75	20/07/2014	14.76	-92.58	80	5		313			231		89		
76	29/07/2014	14.68	-92.69	61	5.3		306	369		234		81	245	
77	28/08/2014	14.18	-92.05	60	5							105		
78	15/10/2014	14.51	-92.7	42	5.1							78		
79	19/11/2014	14.71	-93.39	25	5.2					240		129		
80	04/01/2015	16.29	-94.27	99	5.1					213			173	
81	12/01/2015	15.39	-93.41	82	5.5	326	205	268		190		160	178	305
82	20/01/2015	14.94	-91.55	164	5.5			493						
83	01/03/2015	13.37	-91.01	40	5.3							226		
84	01/05/2015	15.73	93.71	90	5		164	227		186			163	
85	15/05/2015	13.85	-92	11	5.2							124		
86	18/05/2015	14.07	-92.13	62	5.2							114		
87	01/09/2015	15.32	-92.84	108	5.3		265	334		190			197	316
88	17/12/2015	15.76	-93.7	90	6.6		163							
89	14/06/2017	14.77	-92.08	113	7	465						116	274	
90	07/09/2017	14.85	-94.11	58	8.2	273	121	112		272	77			
Total records						10	44	30	57	43	20	24	22	11

* H represents focal depth.

Finally, to suppress site effects from the 261 records, with the ETF computed previously (red continuous line, Figure 3) and the estimated FAS for each record, we compute the deconvolution between the FAS for the nine sites and ETF in the frequency domain for this site, subtracting their respective site effect. The corresponding intensities (spectral acceleration and peak values) are estimated using random vibration theory (RVT) (i.e., Arciniega-Ceballos 1990; Reinoso and Ordaz 1999), which comprises the following steps: (1) de-amplifying the FAS by dividing them by the EHVSR obtaining a proxy of ETF; (2) multiplication of the spectrum by the oscillator transfer function or by one if PGA is seek; (3) calculation of the moments m_0 and m_2 of the power density which are given by $m_k = \int_0^{\infty} \omega^k \, |A(\omega)|.^2 \; d\omega$; (4) estimate the root mean square in terms of m_0 and the strong motion duration, D, for each event; (5) computation of the peak factor F_p, according to RVT, in terms of the number of extrema N occurring during the duration D and from the moments by means of $N=(D/\pi)(m_2/m_0)^{0.5}$, and get the expected peak by multiplying the FAS by F_p. The peak factor is asymptotically given by $F_p = (2\ln N)^{0.5} + 0.577(2\ln N)^{-0.5}$. Regarding D, we use the expression developed by Herrmann (1985), $D = f_c^{-1} + 0.05R$ where f_c= corner frequency (in Hz) and the R=distance (in km). As for response spectral ordinates, both the oscillator transfer function and the additional duration have to be accounted for (see e.g. Boore, 1983).

In this way, the estimated ground motion intensities (e.g. acceleration response spectra) for each event and site will be essentially free of site effect. In Figure 4 this reduction is illustrated for the July 6th, 2007 (M_w=6.2) event. The complex Fourier spectra were deconvolved by the corresponding average EHVSR (ETF) and then transformed back to time domain. The N-S accelerograms of the nine stations are displayed in the left panel. The corresponding distance and PGA are indicated. In the right panel the recordings with suppressed site effect are displayed (as if the corresponding stations were located in hard rock). This suppression gives significantly lower PGA values (for TAJN a factor of 7.5 was obtained). We claim that the use of average EHVSR may be adequate to correct GMPE for site effects, leading to a more realistic attenuation model.

Peak ground accelerations (PGA) are obtained from these corrected records. Also, response spectra with 5 % critical damping are obtained for 24 structural periods ranging between 0.3 and 40 Hz. Finally, peak ground velocities are obtained by integrating these recordings after correcting them for base line (Boore, 2005) and band-pass filtering between 0.3 and 40 Hz.

Each parameter (i.e., PGA, PGV, or the spectral ordinates) is separately calculated for both horizontal components, then the quadratic mean is obtained from both ortogonal components (Boore, 2005). Other alternatives would include the geometric mean, or other no geometrical means (Boore, 2010). We used the quadratic vector mean as it is a common practice in the development of attenuation models, since from the physics point of view it is more rational than other means. All recordings were processed in the same form.

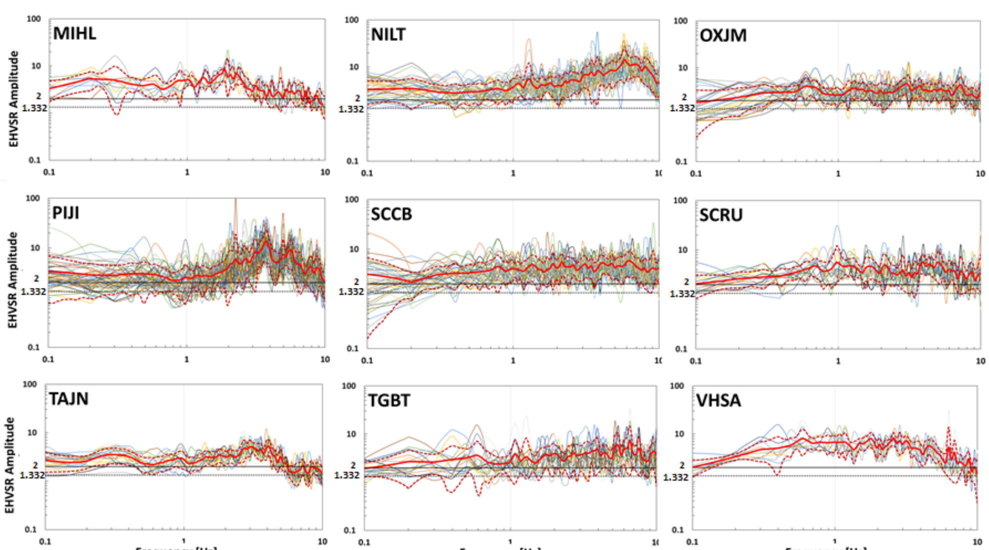

Figure 3. Earthquake horizontal to vertical spectral ratios EHVSR at the nine studied stations. In thin of colours continuous lines, the quadratic mean spectral ratios (continuous red lines) of each earthquake are plotted in log-log scale (dashed red lines: average ± one standard deviation). The trends are clear and the averages at each station, depicted in red, are assumed to represent the site effect. The value of two suggested by SESAME (2000), continuous line, and the theoretical H/V in a Poissonian half-space are given as reference (discontinuous line).

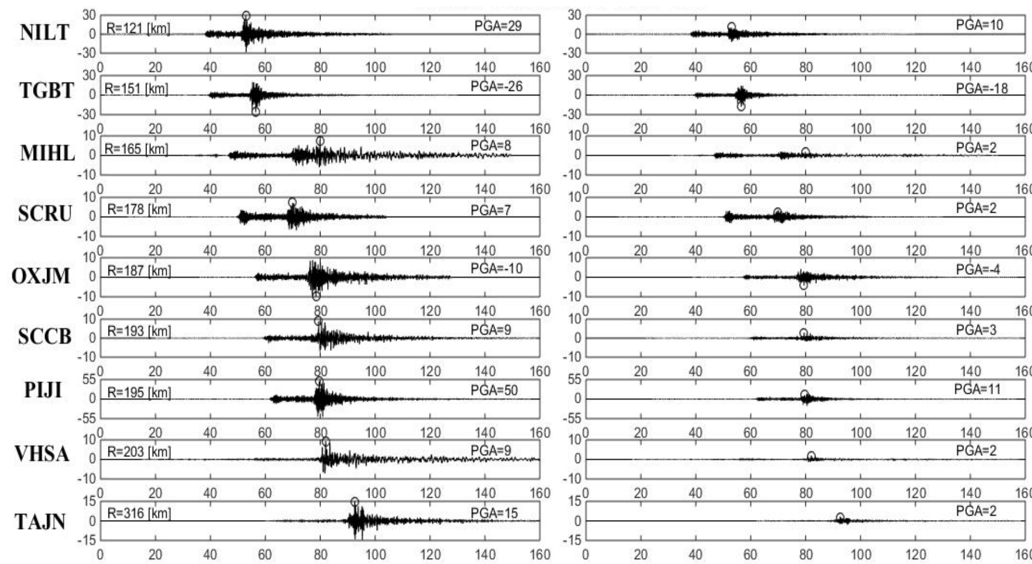

Figure 4. Example of site effects correction for a Mw=6.2 event of July 6th , 2007 for the studied stations. Left panel depicts the N-S accelerations indicating the epicentral distance and the PGA in gals (cm/s2). The right panel shows the time series with the site effects removed with the procedure described herein.

Regression analysis

To estimate the spectral accelerations with a damping of 5 %, as well as the PGA and PGV, the regression analysis of the data set was made using the maximal verisimilitude method of one stage proposed by Boore (1993), which constitutes the most direct form to predict the response spectra of observed data. We use a simpler functional form proposed by Ordaz *et al.* (1989), and García-Soto and Jaimes (2017) to estimate the spectral ordinates, PGA, and PGV for seismic events from southeastern Mexico.

$$lnY(T) = \alpha_1(T) + \alpha_2(T) \cdot M_w + \alpha_3(T) \cdot lnR + \alpha_4(T)R + \varepsilon_1(T) \quad (2)$$

where $Y(T)$ represents the horizontal spectral ordinate based on a quadratic mean of the horizontal components, T in seconds is the period of the single degree of freedom system, Mw is the moment magnitude, *R* is the closest distance from site to fault surface for larger events (Mw > 6.5) or the hypocentral distance for the rest, both in km, $\square_i$ are the coefficients estimated by the regression analysis, and ε_1 is the error estimation by assuming a normal distribution.

Noteworthy is that in previous studies (i.e., Arroyo, 2010; García-Soto and Jaimes, 2017) no important dependence with the focal depth was found, consequently it was not considered in excluded from this study. Even more, the quadratic mean was used since the use of the geometric mean and was the development of the attenuation relationship is slightly less conservative than the use of the quadratic mean to evaluate seismic risk (i.e., Hong and Goda, 2007). The horizontal geometric dispersion can be obtained as $G(R) = R^{\alpha_3(T)}$, where $\alpha_3(T)$ is the geometric attenuation coefficient, which controls the amplitude decay with the distance, R. By applying the natural logarithm to both sides of the last expression, it can be linearized as $ln\big(G(R)\big) = \alpha_3(T) \cdot lnR$, which corresponds to the third term of equation (2). In this study, it was considered that $\alpha_3(T)$ is very well constrained by seismic observations in intraplate events (i.e., Ordaz *et al.* 1994; Reyes, 1999; Jaimes *et al.* 2006; Garcia-

Soto and Jaimes, 2017). Further, by fixing the geometric dispersion coefficient at -0.5 for all the ordinates in both components (i.e., Ordaz *et al.*, 1994; Reyes, 1999; Jaimes *et al.*, 2006), unrealistic values are avoided (i.e., non-negative values of $\alpha_3(T)$,) that physically have no sense (Ordaz *et al.* 1994).

Results and Discussion

Regression Coefficients and Residuals

Regression coefficients, $\alpha_i(T)$, and the standard deviation $\sigma_i(T)$, were estimated for periods T between 0.1 and 10 s, for recordings of 4 groups: Group 1, considers all recordings without site effects; Group 2, includes the recordings with site effects; Group 3, comprises recordings of earthquakes with depths less than 80 km but without site effects; while Group 4, is constituted by recordings of earthquakes with depths less than 250 km and no corrected for site effects. Figure 5 shows, in a logarithmic scale, the values of the regression coefficients $\alpha_1(T)$, $\alpha_2(T)$ and $\alpha_4(T)$ for period values between 0.1 and 10 s. No differences significant are found between coefficients α_2 and α_4 among the 4 groups. However, coefficient α_1 of group 2 (which includes site effects) shows an evident divergence, from the others groups. Confirmation of the validity of the attenuation model is indicated by the standard deviation $\sigma_i(T)$obtained for the cases with and without site effects. Table 2 summarizes the regression coefficients $\alpha_i(T)$ and the standard deviation obtained from the analyzed recordings by considering the quadratic mean of the horizontal components.

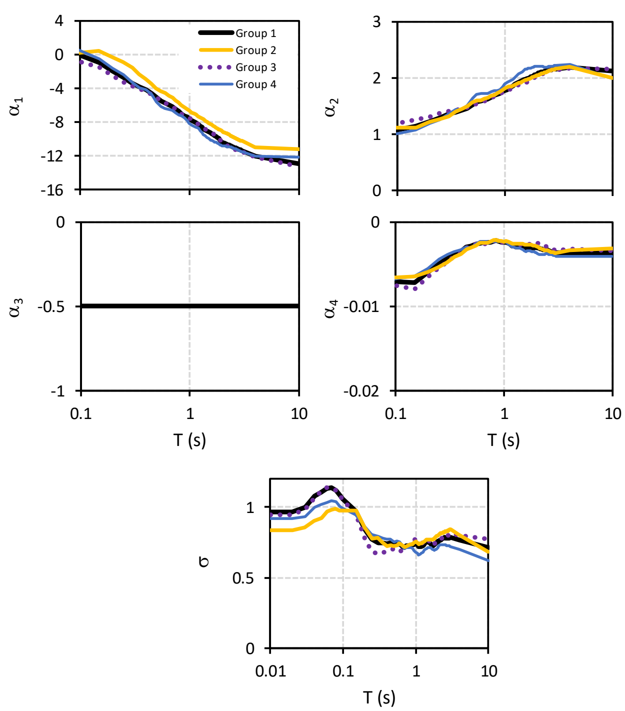

Figure 5.- Regression coefficients and natural logarithmic standard deviation logarithmic for horizontal components in the sites of Chiapas State, Mexico. a) Group 1: all records without site effects. B) Group 2 all records presenting

site effects, c) Group 3 including records with depths less than 80 km, and d) Group 4 with records with depths less than 250 km and no site effect.

For the purpose of this analysis, the residual is defined as:

$$\delta_i = ln(Y_i) - ln(\bar{Y}) \tag{3}$$

where $ln(Y_i)$ is the natural logarithm of i-eth observed value $Y_i$and $ln(\bar{Y})$ is the corresponding predicted value. The attenuation model in order to non-biased estimations, the residual must have a zero mean, and do not present any correlation with the regression model parameters, i.e., the magnitude (Mw) and distance R. Figure 6 shows the residuals δ_i obtained from the regression of the horizontal components as functions of magnitude (upper panel), and of the distance (lower panel) for PGA and spectral ordinates for T= 0.06, 0.5, and 1 s. These figures consider a) all recordings without site effects, b) all recordings with site effects, c) recordings from earthquakes with depths less than 80 km and without site effect, and d) recordings from earthquakes with depths less than 250 km and without site effects. These figures shows that the regression model is not biased neither towards magnitude nor distance. The tendency lines are shown with a thick line.

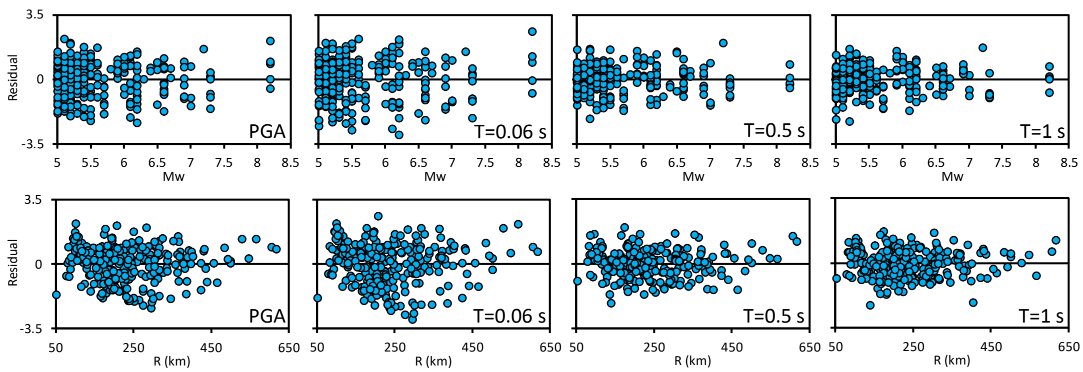

a)

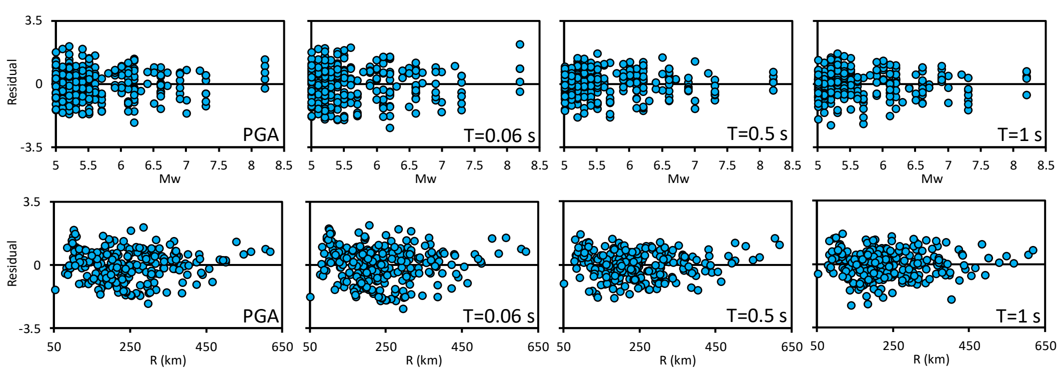

b)

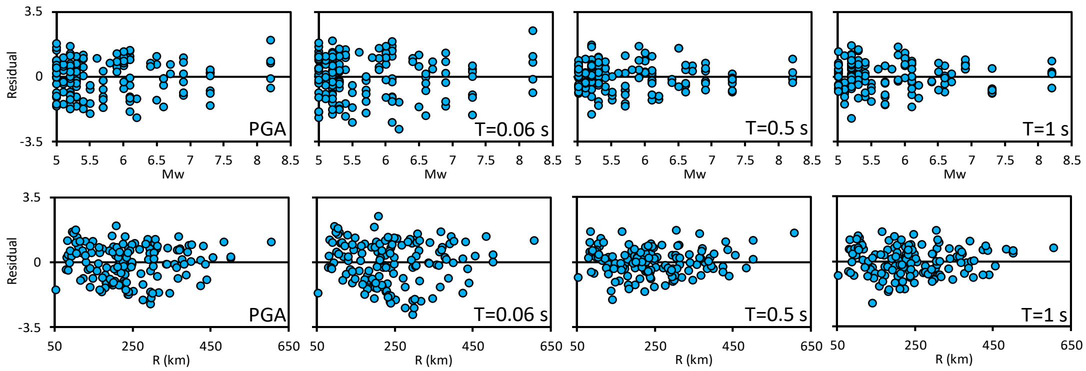

c)

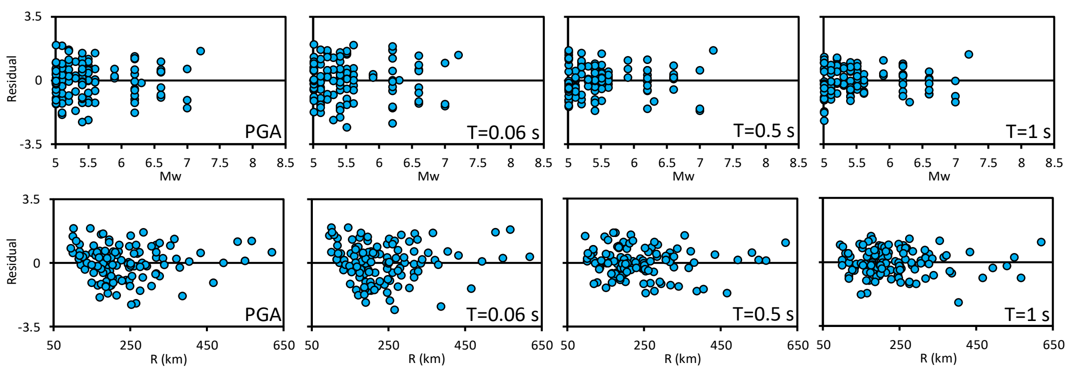

d)

Figure 6. Residual values obtained from the regression of the horizontal components according to magnitude (upper part of panel), and with respect to distance (lower part of each panel) for peak ground acceleration (PGA) and spectral pseudoaceleration, Sa, at T values of 0.06, 0.5, and 1 s. Panel a comprises all records without site effect, panel b includes all records with site effect, panel c considers records with depths less than 80 km and without site effect. Finally, panel d corresponds to records with depth less than 250 without site effect.

Table 2.- Regression coefficients obtained for the horizontal components.

	Group 1				Group 2			
T (s)	α_1	α_2	α_4	α	α_1	α_2	α_4	α
0.01	-1.5508	1.1515	-0.0066	0.96	-1.1789	1.2033	-0.0057	0.84
0.02	-1.5518	1.1516	-0.0066	0.96	-1.1802	1.2036	-0.0057	0.84
0.04	-0.9102	1.1402	-0.0070	1.08	-0.8432	1.2014	-0.0062	0.90
0.06	0.0273	1.0727	-0.0077	1.13	-0.2829	1.1604	-0.0067	0.97
0.08	0.1705	1.0758	-0.0074	1.12	0.0004	1.1415	-0.0067	0.99
0.1	-0.0772	1.0803	-0.0071	1.06	0.2687	1.1119	-0.0065	0.98
0.2	-1.8836	1.2276	-0.0060	0.84	-0.3723	1.2176	-0.0060	0.85
0.3	-3.3412	1.3582	-0.0043	0.75	-1.5325	1.3277	-0.0048	0.78
0.4	-4.1157	1.4207	-0.0036	0.74	-2.8650	1.4583	-0.0039	0.72
0.5	-5.0784	1.5269	-0.0029	0.74	-3.9424	1.5641	-0.0031	0.72
0.6	-5.7386	1.5918	-0.0025	0.74	-4.5830	1.6097	-0.0025	0.74
0.7	-6.1632	1.6285	-0.0025	0.71	-5.0980	1.6559	-0.0025	0.72
0.8	-6.7363	1.6862	-0.0023	0.73	-5.6886	1.7072	-0.0022	0.73
0.9	-7.2001	1.7347	-0.0023	0.74	-6.1589	1.7580	-0.0022	0.74
1	-7.5814	1.7794	-0.0024	0.74	-6.6258	1.8121	-0.0023	0.76
1.1	-7.9202	1.8218	-0.0026	0.72	-6.9805	1.8454	-0.0024	0.74
1.2	-8.2500	1.8662	-0.0029	0.72	-7.2676	1.8767	-0.0026	0.74
1.3	-8.6025	1.9053	-0.0029	0.74	-7.5384	1.9029	-0.0027	0.76
1.4	-8.9040	1.9359	-0.0029	0.75	-7.8037	1.9253	-0.0026	0.77
1.5	-9.1855	1.9686	-0.0030	0.75	-8.0682	1.9535	-0.0026	0.77
1.6	-9.3861	1.9875	-0.0031	0.74	-8.2767	1.9731	-0.0027	0.77
1.7	-9.6182	2.0066	-0.0030	0.73	-8.5064	1.9932	-0.0027	0.77
1.8	-9.8511	2.0287	-0.0030	0.73	-8.7205	2.0161	-0.0028	0.78
1.9	-10.0840	2.0525	-0.0031	0.74	-8.8946	2.0317	-0.0028	0.79
2	-10.3230	2.0783	-0.0030	0.75	-9.0643	2.0470	-0.0029	0.80
2.1	-10.5020	2.1001	-0.0031	0.76	-9.2065	2.0651	-0.0031	0.81
2.2	-10.6030	2.1060	-0.0032	0.77	-9.3423	2.0806	-0.0032	0.81
2.3	-10.6940	2.1132	-0.0033	0.77	-9.4559	2.0931	-0.0033	0.82
2.4	-10.8300	2.1258	-0.0033	0.78	-9.5928	2.1075	-0.0033	0.82
2.5	-10.9520	2.1373	-0.0033	0.78	-9.7241	2.1211	-0.0034	0.83
2.6	-11.0450	2.1454	-0.0034	0.78	-9.8505	2.1347	-0.0035	0.83
2.7	-11.1190	2.1487	-0.0035	0.78	-9.9396	2.1407	-0.0035	0.83
2.8	-11.2020	2.1547	-0.0036	0.78	-10.0500	2.1501	-0.0036	0.83
2.9	-11.2640	2.1582	-0.0036	0.78	-10.1420	2.1582	-0.0036	0.84
3	-11.3170	2.1597	-0.0037	0.78	-10.2080	2.1620	-0.0037	0.84
4	-12.0000	2.1999	-0.0036	0.76	-11.0170	2.2074	-0.0034	0.80
10	-12.9230	2.1268	-0.0037	0.71	-11.2190	2.0019	-0.0031	0.68
PGA	-1.5528	1.1517	-0.0066	0.96	-1.1804	1.2035	-0.0057	0.84
PGV	-7.9782	1.5989	-0.0045	0.69	-5.2675	1.3045	-0.0015	0.72

*Coefficient α_3 was fixed at -0.50 for the horizontal components.

Table 2 (continuation)

	Group 3				Group 4			
T (s)	α_1	α_2	α_4	α	α_1	α_2	α_4	α
0.01	-2.4021	1.2740	-0.0068	0.94	-0.6243	1.0278	-0.0066	0.92
0.02	-2.4032	1.2741	-0.0068	0.94	-0.6255	1.0280	-0.0066	0.92
0.04	-1.9104	1.2753	-0.0070	1.07	0.2756	0.9883	-0.0072	1.00
0.06	-0.9018	1.2115	-0.0081	1.14	0.8888	0.9587	-0.0074	1.03
0.08	-0.7548	1.2182	-0.0079	1.12	1.0427	0.9535	-0.0071	1.04
0.1	-0.8250	1.1929	-0.0075	1.05	0.4859	1.0117	-0.0068	0.99
0.2	-2.4394	1.3187	-0.0066	0.77	-1.6079	1.1957	-0.0055	0.86
0.3	-3.7200	1.4183	-0.0047	0.67	-3.2780	1.3628	-0.0039	0.79
0.4	-4.3712	1.4573	-0.0038	0.68	-4.1248	1.4403	-0.0034	0.77
0.5	-5.0664	1.5030	-0.0027	0.70	-5.5705	1.6473	-0.0030	0.75
0.6	-5.6933	1.5746	-0.0027	0.69	-6.4074	1.7271	-0.0023	0.75
0.7	-6.1841	1.6204	-0.0026	0.70	-6.6099	1.7249	-0.0024	0.71
0.8	-6.7908	1.6798	-0.0023	0.73	-7.0916	1.7708	-0.0023	0.71
0.9	-7.2440	1.7291	-0.0022	0.75	-7.4292	1.7927	-0.0023	0.70
1	-7.4932	1.7537	-0.0024	0.77	-8.1831	1.8992	-0.0023	0.68
1.1	-7.8381	1.7911	-0.0025	0.76	-8.5043	1.9452	-0.0026	0.66
1.2	-8.2195	1.8408	-0.0027	0.74	-8.7325	1.9763	-0.0030	0.67
1.3	-8.5256	1.8707	-0.0028	0.76	-9.1991	2.0367	-0.0031	0.69
1.4	-8.7945	1.8908	-0.0027	0.77	-9.6278	2.0958	-0.0031	0.71
1.5	-9.0462	1.9132	-0.0027	0.77	-9.9370	2.1393	-0.0034	0.71
1.6	-9.2658	1.9325	-0.0028	0.74	-10.1650	2.1670	-0.0035	0.71
1.7	-9.5299	1.9576	-0.0027	0.73	-10.3090	2.1700	-0.0034	0.70
1.8	-9.7789	1.9782	-0.0026	0.74	-10.4910	2.1886	-0.0035	0.69
1.9	-10.0690	2.0087	-0.0026	0.75	-10.6570	2.2050	-0.0036	0.70
2	-10.3500	2.0384	-0.0025	0.76	-10.7930	2.2171	-0.0036	0.72
2.1	-10.5730	2.0661	-0.0026	0.77	-10.8310	2.2162	-0.0038	0.72
2.2	-10.6890	2.0764	-0.0026	0.77	-10.8720	2.2093	-0.0038	0.73
2.3	-10.8370	2.0959	-0.0028	0.78	-10.8630	2.1960	-0.0039	0.73
2.4	-11.0080	2.1167	-0.0029	0.79	-10.9130	2.1914	-0.0038	0.73
2.5	-11.1280	2.1300	-0.0029	0.80	-11.0370	2.2001	-0.0038	0.73
2.6	-11.2220	2.1403	-0.0031	0.80	-11.1400	2.2076	-0.0038	0.73
2.7	-11.3120	2.1481	-0.0032	0.80	-11.1990	2.2063	-0.0038	0.73
2.8	-11.3780	2.1511	-0.0032	0.80	-11.3060	2.2163	-0.0039	0.72
2.9	-11.4150	2.1518	-0.0033	0.81	-11.3910	2.2223	-0.0040	0.73
3	-11.4340	2.1479	-0.0034	0.82	-11.4980	2.2325	-0.0040	0.72
4	-12.0980	2.1843	-0.0032	0.80	-12.0520	2.2499	-0.0041	0.70
10	-13.1860	2.1597	-0.0034	0.77	-12.1180	2.0009	-0.0041	0.62
PGA	-2.4043	1.2743	-0.0068	0.94	-0.6286	1.0285	-0.0066	0.92
PGV	-8.4826	1.6581	-0.0045	0.68	-7.5498	1.5644	-0.0047	0.65

**Coefficient α_3 was fixed at -0.50 for the horizontal components.

Comparison with Other Studies

To the author's knowledge, there are no GMPEs in the region under study, which makes the outcome more necessary to compute the seismic hazard in the region. For that reason, the Figure 7 compares the attenuation model obtained in this study (for magnitudes Mw of 5.5, 6.5, and 7.5) with those of García *et al.*, (2005), Arroyo *et al.*, (2010) and García-Soto and Jaimes (2017), based on earthquakes located at the Pacific Ocean coasts (discontinuous lines). Attenuation models obtained in this study present a slower decay than previous ones, and models that include site effects (yellow lines) present larger amplitudes than those without site effects (black lines).

Previous attenuation models are clearly different to the attenuation models here presented for southeastern Mexico. These differences could be due to the fact that in southeastern Mexico earthquakes attain depths up to about 243 km, while in the Guerrero coast (southern Mexico) depths are less than 80 km. In general, models by Arroyo *et al.* (2010) and Garcia-Soto and Jaimes (2017) follow a similar pattern in all cases, and for Sa, for T = 0.5 s and 1 s, they decay almost in the same way as the model by Garcia (2005) for Mw 5.5 and 6.5. For PGA, the model by Garcia (2005) present larger amplitudes (for the three magnitudes) than those by the models by Arroyo *et al.* (2010) and Garcia-Soto and Jaimes (2017). In particular, the PGA models corrected for site effects (obtained in this study) have smaller amplitudes than the models by Arroyo *et al.* (2010) and Garcia-Soto and Jaimes (2017) only for distances smaller than 130, 90 and 50 km for Mw 5.5, 6.5 and 7.5, respectively. On the contrary, Sa models corrected for site effects present lower amplitudes than those of the previous models. However, and as it was expected, the corresponding models that include site effects (yellow lines) present the largest amplitudes at all distances. In other words, a model comprising site effects presents overestimated values.

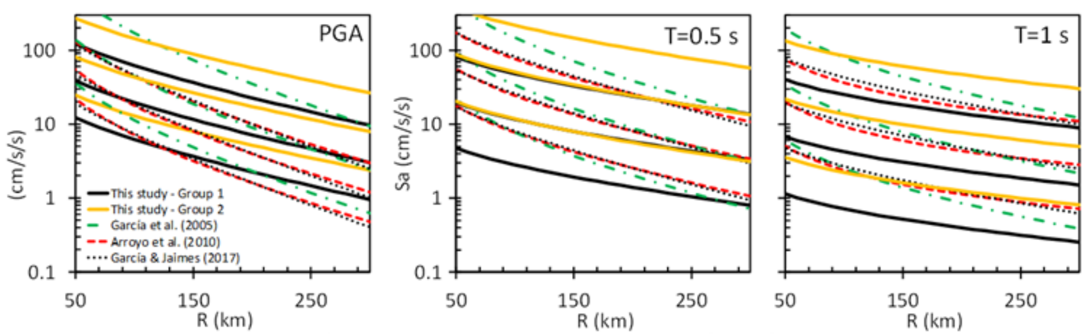

Figure 7. Regression curves for the horizontal component for PGA and spectral pseudo-acceleration, Sa, for periods of 0.5 and 1 s for earthquakes with magnitudes Mw of 5.5, 6.5, and 7.5. Group 1 comprises regression of all records without site effect, while group 2 includes all records with site effect.

CONCLUSIONS

We present an attenuation model for strong motion for southeastern Mexico which is approximately free of local amplification. This means that the GMPE thus obtained can be regarded as appropriate for firm ground. This was accomplished using average EHVSR to construct an empirical transfer function (ETF) for each site to perform a spectral deconvolution on observed records. A statistical regression model was adjusted to construct the corrected GMPE. The model is built as a function of the magnitude and distance from 86 seismic events with magnitudes $5.0 \leq M_w \leq 8.2$, and distances $52 \leq R \leq 618$ km recorded at the states of Chiapas, Oaxaca, Tabasco and Veracruz.

This study shows a practical, approximate approach to remove the site effect in the ground motion attenuation models, the so called GMPE. Otherwise, the seismic intensities could be overestimated. Such is the case in the current values of regulatory norms for the study region. We approximately suppress site effects at the accelerometric stations which provide data to construct attenuation models using the average EHVSR. The aim is to obtain reasonable seismic intensities without the bias induced by local site effects.

Acknowledgements

We thank H. Kawase, S. Matsushima and F. Nagashima for the careful reading of the manuscript and many useful suggestions. Help from J. E Plata and G. Sánchez N. and their team from USI–Instituto de Ingeniería, Universidad Nacional Autónoma de México (UNAM) was crucial to locate some references. Our appreciation to all the technicians who manage, analyze, and give maintenance to the accelerometric network of the Instituto de Ingeniería of the Universidad Nacional Autónoma de México (II-UNAM) installed in the states of Chiapas, Oaxaca, Tabasco, and Veracruz, and that from the SSN. A. L. Ruiz-Gordillo, J. A. Martínez-González and R. Vázquez-Rosas helped us in software work. Thanks are given to J. E. Plata and G. Sánchez of USI, II-UNAM for their multifarious help. Partial support by DGAPA-UNAM, México, under Projects IN100917 and IN107720, is greatly appreciated.

References

Arciniega-Ceballos, A., 1990, Modelo semi-empírico para estimar espectros de respuesta sísmicos en el valle de México, Thesis, Universidad Nacional Autónoma de México.

Arroyo, D., García, D., Ordaz, M., Mora, M. A. and Singh, S. K., 2010, Strong ground-motion relations for Mexican interplate earthquakes, *J. Seismol*, 14(4), 769–785.

Baena-Rivera, M., Perton, M., and Sánchez-Sesma, F. J., 2016, Surface waves retrieval from Generalized Diffuse Fields in 2D synthetic models of alluvial valleys, *Bulletin of the Seismological Society of America*, 106, 2811–2816, doi: 10.1785/0120160084.

Boore, D. M., 1983, Stochastic simulation of high-frequency ground motions based on seismological models of the radiated spectra, *Bulletin of the Seismological Society of America*, 73, 1865-1894

Boore, D. M., 2005, On pads and filters: Processing strong-ground motion data, Bulletin of the Seismological Society of America, 95(2), 745–750.

Boore, D. M., 2010, Orientation-independent, nongeometric-mean measures of seismic intensity from two horizontal components motion, *Bulletin of the Seismological Society of America*, 100(4), 1830-1835.

Carpenter, N. S., Wang, Z., Woolery, E.W. and Rong, M., 2018, Estimating Site Response with Recordings from Deep Boreholes and HVSR: Examples from the Mississippi Embayment of the Central United States, *Bulletin of the Seismological Society of America*, 108(3A), 1199-1209, doi: 10.1785/0120170156.

Finn, W. D. L., 1991, Geotechnical engineering aspects of microzonation, *Proc, Fourth Int, Conf. on Seismic Zonation*, Stanford, California, I, 199-259.

Figueroa J. A., 1973, Sismicidad en Chiapas, Series del Instituto de Ingeniería, Universidad Nacional Autónoma de México, SID 316, pp. 50.

Figueroa, J., Lomnitz, C., Dawson, A., Meli, R. and Prince, J., 1975, Los sismos de julio-octubre de 1975 en el Municipio de Chiapas de Corzo, Chiapas, Instituto de Ingeniería, Universidad Nacional Autónoma de México, Reporte interno, pp. 40.

García, D., Singh, S.K., Herráiz, M., Ordaz, M. and Pacheco, 2005, Inslab earthquakes of Central Mexico: Peak ground-motion parameters and response spectra, *Bull. Seismol. Soc. Am*, 95(6), 2272–2282.

García, D., 2007, Estimación de parámetros del movimiento fuerte del suelo para terremotos intraplaca e instraslab en México central, Ph D.Thesis, Madrid: Universidad Complutense.

García-Soto, A. D., and Jaimes, M. A., 2017, Ground-Motion Prediction Model for Vertical Response Spectra from Mexican Interplate Earthquakes. *Bulletin of the Seismological Society of America*, 107, 887-900.

Gutiérrez, C. and Singh, S. K., 1992, A site effect study in Acapulco, Guerrero, Mexico: comparison of results, *Bull. Seism. Soc. Am*,78, 42-63.

Hennino, R., Tregoures, N., Shapiro, N.M., Margerin, L., Campillo, M., Van Tiggelen B.A. and Weaver, R. L., 2001, Observation of equipartition of seismic waves, Phys. Rev. Lett., 86, 3447–3450. doi: 279 10.1103/*Phys Rev Lett.* 86.3447.

Hermann, R. B., 1985, An extension of random vibration theory estimates of strong ground motion to large distance, *Bulletin of the Seismological Society of America*, 7, 157-171.

HIC-AL, 2017, Reporte periodístico del 15 de septiembre del 2017, realizado por el Grupo de trabajo sobre producción y gestión social de Hábitat-HIC-AL, 2017.

Hong, H., and Goda, K., 2007, Orientation-dependent ground-motion measure for seismic-hazard assessment, *Bull. Seismol. Soc. Am*, 97(5), 1525 - 1538.

Jaimes, M. A., Reinoso, E., and Ordaz, M., 2006, Comparasion of methods to predict response spectra at instrumented sites given the magnitude and distance of an earthquake, *Journal of Earthquake Engineering*, 10(6), 887-902.

Joyner, W. B., and Boore, D. M., 1993, Methods for regression analysis of strong-motion data, *Bulletin of the Seismological Society of America*, 83**(**2), 469–487.

Kawase, H., Sánchez-Sesma, F. J. and Matsushima, S., 2011, The optimal use of horizontal-to-vertical (H/V) spectral ratios of earthquake motions for velocity structure inversions based on diffuse field theory for plane waves, *Bulletin of the Seismological Society of America*, 101(5), 2001-2014, doi: 10.1785/0120100263.

Kawase, H. Mori, Y. and Nagashima F., 2018, Difference of horizontal-to-vertical spectral ratios of observed earthquakes and microtremors and its application to S-wave velocity inversion based on the diffuse field concept, *Earth, Planets and Space*, 70, 32p, https://doi.org/10.1186/s40623-017-0766-4

Kostoglodov, V., and Pacheco, J., 1999, Cien años de sismicidad en México. Ciudad de México: Instituto de Geofísica, Universidad Nacional Autónoma de México.

Lachet, C. and Bard, P. Y., 1994, Numerical and theoretical investigations on the possibilities and limitations of Nakamura's technique, *J. Phys. Earth.*, 42, 377-397.

Lermo, J. and Chávez-García, F. J., 1993, Site effect evaluation using spectral ratios with only one station. *Bulletin of the Seismological Society of America*, 83, 1574-1594.

Lermo, J. and Chávez-García, F. J., 1994a, Site effect evaluation at Mexico City. Dominant period and relative amplification from strong motion and microtremors records, *Soil Dyn. & Earthq. Eng.*, 13, 413-423.

Lermo, J. and Chávez-García, F. J., 1994b, Are microtremors useful in site response evaluation? *Bull. Seism. Soc. Am.*, 84, 1350-1364.

Margerin, L., 2009, Generalized eigenfunctions of layered elastic media and application to diffuse fields, *J. Acoust. Soc. Am.*, 125, 164-174.

Margerin, L., Campillo, M., Van Tiggelen, B. A., and Hennino, R., 2009, Energy partition of seismic coda waves in layered media: Theory and application to Pinyon Flats Observatory, *Geophys. J. Int.*, 177, 571–585.

Martínez-González, J.A., Lermo J., Sánchez-Sesma, F.J., Angulo-Carrillo, J., Valle-Orozco, R., Ordoñez-Alfaro, J., Pérez-Rocha L.E., 2012, Effects of the subsidence on the changes of dominant periods of soils within Mexico City Valley. In: 15th World Conference on Earthquake Engineering id.3598.

Martínez-González, J.A., Lermo J., Vergara-Huerta, F., Ramos-Pérez, E., 2015, Avances en la zonificación sísmica de la ciudad de México y zona de Chalco, Edo. de Mex., propuesta de nuevo mapa de periodos dominantes para las NTC para diseño por sismo del reglamento del D.F. In: XX Congreso Nacional de Ingeniería Sísmica, Sociedad Mexicana de Ingeniería Sísmica.

Nakamura, Y., 1989, A method for dynamic characteristics estimation of subsurface using microtremor on ground surface. Quarterly Report of the Railway Technical Research Institute. QR RTRI 30 (1), 25-33.

Ordaz, M., Jara, J. and Singh, K. S., 1989, Riesgo sísmico y espectros de diseño en el EstadodeGuerrero, Memoria del VIII Congreso Nacional de Ingeniería Sísmica, México, D40-D56.

Ordaz, M., Singh, S. K., and Arciniega, A., 1994, Bayesian attenuation regressions: an application to Mexico City. *Geophysical Journal International*, 117(2), 335-344.

Pérez-Yañez, C., Ramírez-Guzmán, L., Ruíz G.A.L., Delgado, D.R., Macias, C.M.A., Sandoval, G. H., Quiróz R. A. (14-19 de Diciembre de 2010), Strong Ground Motion Database System for Mexican Seismic. San Fransisco: AGU Fall Meeting.

Rebollar, C. J., Quintanar, L., Yamamoto, J., and Uribe, A., 1999, Source Process of the Chiapas, Mexico, Intermediate-Depth Earthquake (Mw=7.2) of 21 October 1995, *Bulletin of the Seismological Society of America*, 89, 348-358.

Reinoso, E., and Ordaz, M., 1999, Spectral ratios for Mexico City from free-field recordings, *Earthquake Spectra*, 15, 273-295.

Reyes, C., 1999, El estado límite de servicio en el diseño sísmico de edificios, Ph.D. Tesis, UNAM, México.

Sánchez-Sesma, F. J., and Campillo, M., 2006, Retrieval of the Green's function from cross-correlation: The canonical elastic problem, *Bulletin of the Seismological Society of America*, 96, 1182-1191.

Sánchez-Sesma, F. J., Pérez-Ruiz, J. A., Campillo, M. and Luzón, F., 2006, Elastodynamic 2D green function retrieval from cross-correlation: Canonical inclusion problem, *Geophys. Res. Lett.*, 33, L13305-1-6.

Sánchez-Sesma, F. J., Pérez-Ruiz, J. A., Luzón, F., Campillo, M., and Rodríguez-Castellanos, A., 2008, Diffuse fields in dynamic elasticity, *Wave Motion*, 45, 641-654.

Sánchez-Sesma F.J., Weaver R.L., Kawase H., Matsushima S., Luzón F., and Campillo M., 2011a, Energy Partitions among elastic waves for dynamic surface loads in a semi-infinite solid, *Bulletin of the Seismological Society of America*, 101(4), 1704-1709, doi: 10.1785/0120100196.

Sánchez-Sesma, F. J., Rodríguez, M., Iturrarán-Viveros, U., Luzón, F., Campillo, M., Margerin, L., García-Jerez, A., Suárez, M., Santoyo, M. A. & Rodríguez-Castellanos, A., 2011b, A theory for microtremor H/V spectral ratio: application for a layered medium, *Geophys. J. Int.*, 186, 221-225. doi: 10.1111/j.1365-246X.2011.05064.

SSN, 1993, Reporte de sismo:10 de Septiembre de 1993 (Mw7.2), Servicio Sismologico Nacional (SSN), Instituto de Geofísica, Universidad Nacional Autónoma de México, pp 5.

SSN, 2012, Reporte de sismo: Sismo del día 7 de Noviembre de 2012, Chiapas (Mw7.3), Servicio Sismologico Nacional (SSN), Instituto de Geofísica, Universidad Nacional Autónoma de México, pp 5.

SSN, 2017, Reporte Especial: Sismo de Tehuantepec, 7 de septiembre de 2017 (M 8.2), Servicio Sismologico Nacional (SSN), Instituto de Geofísica, Universidad Nacional Autónoma de México, pp 11.

Weaver, R. L., 1982, On diffuse waves in solid media, *Journal of the Acoustic Society of America*, 71, 1608-1609.

Weaver, R. L., 1985, Diffuse elastic waves at a free surface, *Journal of the Acoustic Society of America*, 78, 131-136.

Weber, B., Schaaf, P., Valencia, V. A., Iriondo, A., and Ortega-Gutierrez, F., 2006, Provenance ages of late Paleozoic sandstones (Santa Rosa Formation) from the Maya Block, SE México: implications on the tectonic evolution of western Pangea, *Revista mexicana de ciencias geológicas*, 23(3), 262-276.

Ye, L., Lay, T., Bai, Y., Cheung, K. F., & Kanamori, H., 2017, The 2017 Mw 8.2 Chiapas, Mexico, earthquake: Energetic slab detachment. *Geophysical Research Letters*, 44, 11,824–11,832. https://doi.org/10.1002/2017GL076085.